CHEMISTRY OF MATERIALS

Article

pubs.acs.org/cm

Zeta Potential for Metal Oxide Nanoparticles: A Predictive Model Developed by a Nano-Quantitative Structure–Property Relationship Approach

Alicja Mikolajczyk,[†] Agnieszka Gajewicz,[†] Bakhtiyor Rasulev,[‡,§] Nicole Schaeublin,[∥] Elisabeth Maurer-Gardner,[∥] Saber Hussain,[∥] Jerzy Leszczynski,[‡] and Tomasz Puzyn*[,†]

[†]Laboratory of Environmental Chemometrics, Institute for Environmental and Human Health Protection, Faculty of Chemistry, University of Gdansk, 80-308 Gdansk, Poland

[‡]Interdisciplinary Nanotoxicity Center, Department of Chemistry and Biochemistry, Jackson State University, Jackson, Mississippi 39217-0510, United States

[§]Center for Computationally Assisted Science and Technology, North Dakota State University, NDSU Research Park Drive, Post Office Box 6050, Fargo, North Dakota 58108, United States

[∥]Biological Interaction of Nanomaterials, Applied Biotechnology Branch, Human Effectiveness Directorate 711th, Human Performance Wing, Air Force Research Laboratory, Wright Patterson Air Force Base, Ohio 45433, United States

Supporting Information

ABSTRACT: Physico–chemical characterization of nanoparticles in the context of their transport and fate in the environment is an important challenge for risk assessment of nanomaterials. One of the main characteristics that defines the behavior of nanoparticles in solution is zeta potential (ζ). In this paper, we have demonstrated the relationship between zeta potential and a series of intrinsic physico–chemical features of 15 metal oxide nanoparticles revealed by computational study. The here-developed quantitative structure–property relationship model (nano-QSPR) was able to predict the ζ of metal oxide nanoparticles utilizing only two descriptors: (i) the spherical size of nanoparticles, a parameter from numerical analysis of transmission electron microscopy (TEM) images, and (ii) the energy of the highest occupied molecular orbital per metal atom, a theoretical descriptor calculated by quantum mechanics at semiempirical level of theory (PM6 method). The obtained consensus model is characterized by reasonably good predictivity (Q^2_{EXT} = 0.87). Therefore, the developed model can be utilized for in silico evaluation of properties of novel engineered nanoparticles. This study is a first step in developing a comprehensive and computationally based system to predict physico–chemical properties that are responsible for aggregation phenomena in metal oxide nanoparticles.

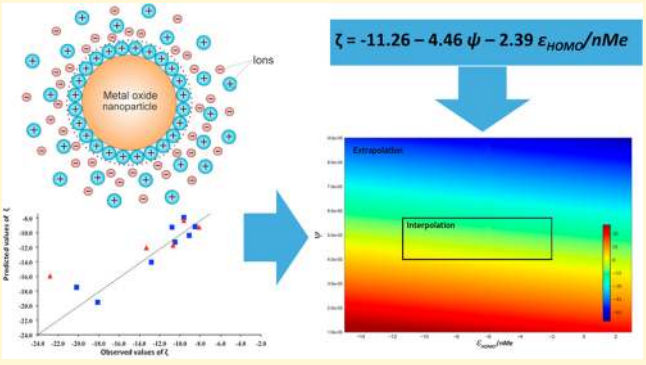

INTRODUCTION

Apart from the many benefits related to wide application of nanomaterials in every-day-life products, rapidly developing nanotechnology may result in many serious threats such as environmental contamination and possible human health problems. Thus, the designing of new nanomaterials should be always accompanied by a comprehensive risk assessment.[1]

Toxicity of nanoparticles to living organisms depends on various structural features (intrinsic properties), such as chemical composition, crystalline form, size, shape, porosity, surface area, and surface chemistry.[2] According to changes in the dispersing environment, nanoparticles can rapidly agglomerate and, in effect, form particles having large diameters. On the contrary, when an organism uptakes an agglomerate of nanoparticles from the environment, depending on the biological conditions (mainly pH) the agglomerate may dissociate and, like a Trojan horse, become a source of much smaller (often also more toxic) particles in the body.[3] Thus, the agglomeration phenomenon largely influences toxicity of nanoparticles.[4] Such properties of nanoparticles that describe their behavior are known as extrinsic properties.

The ease of formation of agglomerates strongly depends on the surface charge that stabilizes dispersed nanoparticles and prevents them from agglomeration. However, the available experimental techniques are unable to measure surface charge directly; its value can only be estimated by measuring zeta potential (ζ) in a given medium.[4b] Therefore, zeta potential (in the limit of $\zeta \pm 30$ eV) is an extremely important parameter in

Received: December 1, 2014
Revised: March 5, 2015

DOI: 10.1021/cm504406a
Chem. Mater. XXXX, XXX, XXX–XXX

Table 1. Sumary Characterization of Data Used in the Study

MeOx-NPs	particle size (nm)	size in media (nm)	spherical size (ψ)	$\varepsilon_{HOMO}/n_{Me}$ (eV)	observed ζ (mV)
V_2O_3	n/a	433.9 ± 40.1	5.20×10^{-05}	−2.5	−22.8
Al_2O_3	44.0	372.3 ± 17.9	5.44×10^{-05}	−4.3	−20.2
Fe_2O_3	32.0	297.6 ± 6.9	5.63×10^{-05}	−4.5	−18.1
Sb_2O_3	90.0−210.0	640.3 ± 77.9	4.95×10^{-05}	−4.0	−13.3
La_2O_3	46.0	672.9 ± 79.1	5.21×10^{-05}	−5.5	−12.8
ZnO	71.0	188.9 ± 37.2	5.15×10^{-05}	−11.4	−10.8
Y_2O_3	38.0	1222.9 ± 351.7	4.80×10^{-05}	−2.0	−10.7
SnO_2	46.1	264.9 ± 64.9	5.06×10^{-05}	−7.0	−10.5
In_2O_3	29.8	224.3 ± 63.1	4.69×10^{-05}	−5.2	−9.6
TiO_2	42.3	1307.0 ± 313.7	4.77×10^{-05}	−7.1	−9.6
WO_3	30.0−70.0	179.6 ± 63.2	5.19×10^{-05}	−10.4	−9.1
ZrO_2	46.7	661.4 ± 14.4	4.99×10^{-05}	−8.9	−8.5
SiO_2	15.0	809.7 ± 97.4	4.89×10^{-05}	−7.1	−8.1
CoO	<100	257 ± 11.9	4.52×10^{-05}	−9.2	−3.4
Bi_2O_3	90.0	2029 ± 150.7	4.16×10^{-05}	−4.5	−2.3

determining stability of nanoparticles in complex media. Theoretical and experimental results have confirmed that zeta potential is affected not only by the suspension conditions, such as pH, temperature, ionic strength, and even the types of ions, but also by the intrinsic particle properties such as size and concentration.[4b,5]

Zeta potential has been used to diagnose cellular interaction with charged ions or molecules. It was shown that the presence of negatively charged ions or molecules decreases the surface zeta potential and that on the contrary the presence of positively charged ions increases the surface zeta potential.[6]

There are also additional factors influencing agglomeration/aggregation phenomena that come into play when serum is introduced to the cell culture media. The proteins in the serum can both discourage agglomeration of some nanoparticles after dispersion[4a] as well as cause nanoparticle agglomeration because of the adsorption of serum proteins onto the surface.[4c] The formation of the corona is a complex and dynamic phenomenon, which requires considerably more research in order to elucidate not only the factors that contribute to its formation but also how it may affect the agglomeration of nanoparticles.

Numerous studies have attempted to address the characterization and evaluation of nanoparticle behavior experimentally. Experimental evaluation of nanoparticle interactions with biological systems is expensive and time-consuming. Thus, there is an increased interest in the application of faster and much less expensive computational techniques such as quantitative structure−property relationship (QSPR) models. The use of QSPR not only eliminates the need of extensive experimental testing but also provides valuable suggestions on the mechanism of the studied phenomena at the molecular level.[1,7] Our group previously investigated various nanoparticles' properties, and developed efficient nano-QSAR and nano-QSPR models.[1,7b,c,8]

In this work, we applied the nano-QSPR approach together with novel nanostructural descriptors derived from transmission electron microscopy (TEM) images to describe relationships between zeta potential (ζ) and structural features of 15 metal oxide nanoparticles (MeOx-NPs).

EXPERIMENTAL SECTION

Nanoparticles and Characterization. Data contained the experimental values of zeta potential (end point) of selected 15 MeOx-NPs (Table 1) that were acquired from our previous study where human keratinocyte cell line (HaCaT) was investigated.[8d]

To verify morphology and size, one drop of a 100 μg/mL solution (RPMI-1640 media, at pH 7.5 (ATCC, Manassas, VA) supplemented with 10% (v/v) fetal bovine serum (FBS, ATCC) and 1% (w/v) penicillin/streptomycin (Sigma, St. Louis, MO) was spotted on a forever/carbon-coated TEM grid (EMS Diasum, Hatfield, PA) and allowed to dry.

Once dried, the nanoparticles were viewed using a Hitachi H-7600 TEM (Schaumburg, IL) at 120 kV. Dynamic light scattering (DLS) for characterization of nanoparticle size and zeta potential (ζ) in cell culture media (serum-free) was done using a Malvern Instruments zeta-sizer Nano-ZS instrument according to the procedure described by Murdock et al.[4a] The details can be found in ref 8d.

Descriptors Calculation. Each of 15 metal oxide nanoparticles was characterized by a series of 28 descriptors, including 11 microscopic-image-based and 17 theory-based (calculated) descriptors.

The first group of 11 descriptors has been derived from images obtained with Hitachi H-7600 TEM capable of 0.35 nm point-to-point resolution. Each image has been converted to numerical format, by converting pixels to certain values. In the 8-bit monochrome image (called gray scale image), each pixel has been assigned a value from 0 to 255. The assigned values depend on the image gray levels (255 is the total blackness, whereas 0 represents the lowest level). With use of in-house-developed algorithms,[8c] we calculated descriptors related to size distribution, agglomeration state, shape, porosity, and surface area of the studied MeOx-NPs.

Then, the next 17 theoretical quantum−mechanical descriptors were calculated at the semiempirical level of theory with the use of PM6 method implemented in MOPAC2009 software.[9] These calculations were carried out on simplified molecular models of the studied nanoparticles' surface (molecular clusters). The clusters were constructed by employing XP software.[10] All necessary crystallographic data have been collected from Cambridge Crystallographic Data Center (CCDC)[11] and reported in the Supporting Information in Table S1.

The quantum−mechanical calculations included two steps: (i) optimization of the cluster's geometry with respect to the decreasing energy gradient and (ii) calculation of the descriptors on the basis of the optimized geometry. The calculated descriptors (i.e., energy of the highest occupied molecular orbital, energy of the lowest unoccupied molecular orbital, electronic energy, and total energy) describe electronic properties of the MeOx-NPs. Nanostructural descriptors (Table S2 in Supporting Information) have been subjected to an autoscaling operation of which all average values were equal to 0, whereas all variances were equal to 1.

In Figure 1 is represented the distribution of values for two descriptors: spherical size (ψ) and quantum−mechanical ($\varepsilon_{HOMO}/n_{Me}$) by utilizing star diagrams. It can be seen that the distribution of these values is quite different between descriptors.

Data Set Splitting. The data related to the 15 MeOx-NPs were split into two sets: a training set (to be used to develop a nano-QSPR model)

DOI: 10.1021/cm504406a
Chem. Mater. XXXX, XXX, XXX−XXX

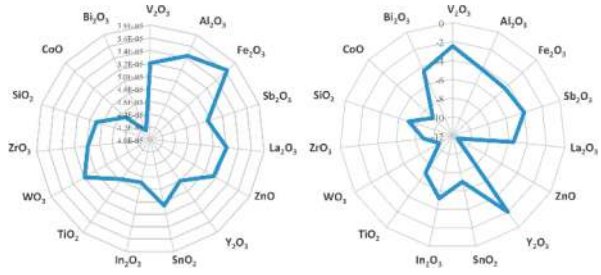

Figure 1. Representation of the distribution of spherical size (ψ) and $\varepsilon_{HOMO}/n_{Me}$ descriptor values using star diagrams (left and right, respectively).

and a validation set (to be used only for validating the model's predictive ability). To perform a splitting, the nanoparticles were sorted along with the increasing values of zeta potential. Then, every third NP was included in the validation set (V), whereas the remaining NPs formed the training set (T). Because models developed on the basis of very small data sets might not be robust enough, we have carried out multiple splittings to investigate the potential influence of the splitting procedure on the modeling results.[8f] Because two metal oxides (TiO_2 and In_2O_3) were characterized by the same values of zeta potential (−9.6 mV), we carried out two additional combinations of the prepared splits (Table 2).

Nano-QSPR model development. In the present study, QSARINS[12] software has been used to develop nano-QSPR models. For every split, we developed a separate nano-QSPR model with multiple linear regression (MLR) technique.[13] In MLR, the end point ($\mathbf{y}_i$) is described as the best combination of the most relevant autoscaled descriptors used as independent variables ($\mathbf{x}_1$, $\mathbf{x}_2$, ..., $\mathbf{x}_n$), expressed as

$$\mathbf{y}_i = b_0 + b_1\mathbf{x}_1 + b_2\mathbf{x}_2 + ... + b_n\mathbf{x}_n \quad (1)$$

The best combination of the most relevant descriptors was selected with use of the genetic algorithm (GA)[14] implemented in the QSARINS software. Figure 2 summarizes the methodological steps carried out for the development of each model.

We used the correlation coefficient (R^2, eq 2) and the root-mean-square error of calibration (RMSEC, eq 3) as the measures of goodness-of-fit for each developed model.

$$R^2 = 1 - \frac{\sum_{i=1}^{n}(y_i^{obs} - y_i^{pred})^2}{\sum_{i=1}^{n}(y_i^{obs} - \tilde{y}^{obs})^2} \quad (2)$$

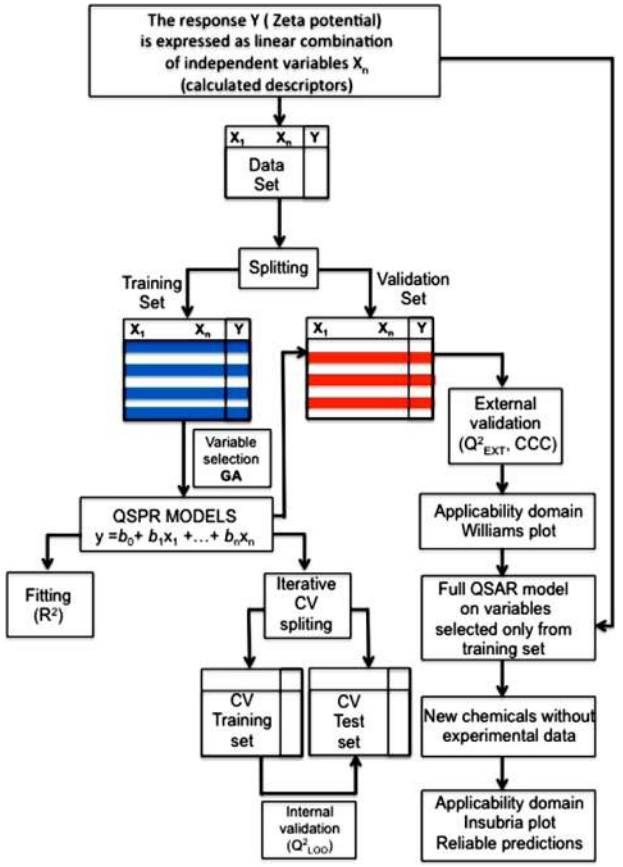

Figure 2. Detailed procedure of developing nano-QSPR models.

$$\mathrm{RMSEC} = \sqrt{\frac{\sum_{i=1}^{n}(y_i^{obs} - y_i^{pred})^2}{n}} \quad (3)$$

where y_i^{obs} is the experimental (observed) value of the property for the ith compound from the training set, y_i^{pred} is the predicted value for ith compound from the training set, $\tilde{y}^{obs}$ is the mean experimental value of the property in the training set, and n is the number of compounds in the training set.

Table 2. Scheme of Data Spliting Towards the Development of Nano-QSPR Models[a]

	split for In_2O_3 in the validation set				split for TiO_2 in the validation set			
MeOx-NPs	split 0	split 1	**split 2**	split 3	split 0	split 1	**split 2**	split 3
V_2O_3	V	T	T	V	V	T	T	V
Al_2O_3	T	T	V	T	T	T	V	T
Fe_2O_3	T	V	T	T	T	V	T	T
Sb_2O_3	V	T	T	V	V	T	T	V
La_2O_3	T	T	V	T	T	T	V	T
ZnO	T	V	T	T	T	V	T	T
Y_2O_3	V	T	T	V	V	T	T	V
SnO_2	T	T	V	T	T	T	V	T
In_2O_3	T	$V_{In_2O_3}$	T_{2O_3}	T	T	V_{TiO_2}	T_{2O_3}	T
TiO_2	V_{In_2O3}	T	T_{TiO_2}	V_{2O_3}	V_{TiO_2}	T	T_{TiO_2}	V_{TiO_2}
WO_3	T	T	V	T	T	T	V	T
ZrO_2	T	V	T	T	T	V	T	T
SiO_2	T	T	T	V	T	T	T	V
CoO	V	T	V	T	V	T	V	T
Bi_2O_3	T	V	T	T	T	V	T	T

[a]T = training set, V = validation set.

DOI: 10.1021/cm504406a
Chem. Mater. XXXX, XXX, XXX−XXX

Table 3. Summary of Single Models and the Consensus Model Developed within This Work

model id	MeOx- NPs[a]	obj. tr.	obj. test	descriptors	R^2	Q^2_{LOO}	Q^2_{EXT}	CCC	RMSEC	RMSCV	RMSEP	b_0	b_1	b_2
0	TiO_2	10	5	ψ, $\varepsilon_{HOMO}/n_{Me}$	0.92	0.81	0.74	0.96	1.38	2.12	3.23	−11.00	−4.70	−4.61
0	In_2O_3	10	5	ψ, $\varepsilon_{HOMO}/n_{Me}$	0.91	0.81	0.74	0.95	1.43	2.14	3.25	−11.00	−4.61	−1.72
1	TiO_2	10	5	ψ, $\varepsilon_{HOMO}/n_{Me}$	0.86	0.69	0.76	0.91	2.0	3.01	2.46	−12.05	−3.76	−3.15
1	In_2O_3	10	5	ψ, $\varepsilon_{HOMO}/n_{Me}$	0.85	0.67	0.81	0.93	2.08	3.13	2.19	−12.05	−3.60	−3.06
2		10	5	ψ, $\varepsilon_{HOMO}/n_{Me}$	0.82	0.55	0.92	0.96	2.26	3.61	1.54	−11.38	−4.74	−2.48
3	TiO_2	10	5	ψ, $\varepsilon_{HOMO}/n_{Me}$	0.94	0.86	0.62	0.72	1.33	2.01	3.22	−10.53	−5.01	−1.96
3	In_2O_3	10	5	ψ, $\varepsilon_{HOMO}/n_{Me}$	0.93	0.85	0.62	0.71	1.39	2.05	3.23	−10.53	−4.95	−1.8
cons.		10	5	ψ, $\varepsilon_{HOMO}/n_{Me}$	0.82		0.87	0.96	2.40		1.25	−11.26	−4.46	−2.39

[a]Models with combination of either TiO_2 or In_2O_3 metal oxide in test set

To verify the stability of the models (sensitivity on the composition of the selection of the training set), in each case we calculated the cross-validated coefficient Q^2_{LOO} (leave-one-out method) and root-mean-square error of cross-validation (RMSECV). Both statistics were calculated according to eqs 4 and 5, represented as

$$Q^2_{LOO} = 1 - \frac{\sum_{i=1}^{n} (y_i^{obs} - y_i^{predcv})^2}{\sum_{i=1}^{n} (y_i^{obs} - \tilde{y}^{obs})^2} \quad (4)$$

$$RMSECV = \sqrt{\frac{\sum_{i=1}^{n} (y_i^{obs} - y_i^{predcv})^2}{n}} \quad (5)$$

where y_i^{obs} is the experimental (observed) value of the property for the ith compound, y_i^{predcv} is the cross-validated predicted value for ith compound, $\tilde{y}^{obs}$ is the mean experimental value of the property in the training set, and n is the number of compounds in the training set.

Following the recommendations by Gramatica and Lin,[15] we calculated the concordance correlation coefficient (CCC, eq 6) as a more restrictive parameter for expressing external predictivity of each model than the commonly used external validation coefficient (Q^2_{EXT}, eq 7) and root-mean-square error of prediction (RMSEP, eq 8). In this work, we applied all three statistics.

$$CCC = \frac{2 \sum_{j=1}^{k_{EXT}} (y_j^{obs} - \hat{y}^{obs})(y_j^{pred} - \hat{y}^{pred})}{\sum_{j=1}^{k_{EXT}} (y_j^{obs} - \hat{y}^{obs})^2 + \sum_{j=1}^{k_{EXT}} (y_j^{pred} - \hat{y}^{pred})^2 + k_{EXT}(\hat{y}^{obs} - \hat{y}^{pred})^2} \quad (6)$$

$$Q^2_{EXT} = 1 - \frac{\sum_{j=1}^{k} (y_j^{obs} - y_j^{pred})^2}{\sum_{j=1}^{k} (y_j^{obs} - \hat{y}^{obs})^2} \quad (7)$$

$$RMSEP = \sqrt{\frac{\sum_{j=1}^{k} (y_j^{obs} - y_j^{pred})^2}{k}} \quad (8)$$

where y_j^{obs} is the experimental (observed) value of the property for the jth compound from the validation set, y_j^{pred} is the predicted value for jth compound from the validation set, $\hat{y}^{obs}$ is the mean experimental value of the property in the validation set, and k is the number of compounds in the validation set.

In addition, we applied the leverage approach and Williams plot to assess the applicability domain (AD) of the finally selected models. This was done to verify the space defined by structural similarity of nanoparticles and the values of zeta potential in which the model can make predictions with the most optimal reliability.[16]

Consensus Modeling. Consensus modeling combines the results of multiple individual models (called member models hereafter), which are constructed by choosing the different training subsets from the whole training set.[17] The basic idea of consensus modeling is that multiple models will effectively identify and encode more aspects of the relationship between independent and dependent variables than will be possible using a single model. It has the advantage of reducing dependence on single sample to obtain prediction results by randomly altering the training set. Therefore, it can be expected to solve overfitting problems caused by the small training set and thereby enhance the stability of the predictions. Theoretically, the error of consensus model $\bar{b}_0(\vec{x})$ can be represented as in ref 7a:

$$b_0\vec{x} = \bar{b}_1(\vec{x}) - \bar{b}_2(\vec{x}) \quad (9)$$

where $\bar{b}_1(\vec{x})$ is the average error across all member models and $\bar{b}_2(\vec{x})$ is the variance of the member models in respect to the results of the consensus model. These two terms are expressed respectively as

$$\bar{b}_1(\vec{x}) = \frac{1}{N_m} \sum_{i=1}^{N_m} (y - \hat{y}_i)^2 \quad (10)$$

$$\bar{b}_2(\vec{x}) = \frac{1}{N_m} \sum_{i=1}^{N_m} (\hat{y}_i - \hat{y})^2 \quad (11)$$

where N_m is the number of the model, $x\rightharpoonup$ is the vector of the independent variables, y is the dependent variable, $\hat{y}_i$ is the prediction result of the ith member model, and $\hat{y}$ is the prediction of the consensus model, which is obtained by averaging of the prediction results of multiple member models by the equation represented as

$$\hat{y} = \frac{1}{N_m} \sum_{\alpha=1}^{Nm} \hat{y}_i \quad (12)$$

In the application of GA to seven data set splits (Table 2), we have created seven individual nano-QSPR models. Then, we used the obtained models to perform consensus modeling. We developed a single consensus model as a combination of all models' coefficients ($\bar{b}_0$, $\bar{b}_1$, $\bar{b}_2$). The goodness-of-fit and prediction ability of the consensus model were estimated on a single training and test set (for split 2, where both of NPs are in training data set, see Table 2).

RESULTS AND DISCUSSION

In the present study, we have developed a consensus nano-QSPR model predicting zeta potential (ζ) for 15 MeOx-NPs that is based on seven models with different splits. The models were developed in accordance to OECD QSAR recommendations.[18] Each of the models is based on the same two molecular descriptors, namely: spherical size (ψ) and the weighted energy of the highest occupied molecular orbital ($\varepsilon_{HOMO}/n_{Me}$).

Their goodness-of-fit measured by the regression coefficient (R^2) is high; it ranges between 82 and 94% (Table 3 and Figure S3 in Supporting Information). However, the indicators of stability (Q^2_{LOO}) and predictive power (Q^2_{EXT} and CCC) of the particular models vary, depending on the split (55% < Q^2_{LOO} < 86%; 62% < Q^2_{EXT} < 92%; 71% < CCC < 96%). Although the variation is within a reasonable robustness range, it indicates that the model is sensitive to the way of splitting data. This is because an individual nano-QSPR model developed with a limited number of data points might ignore and/or underestimate some important information.[17] Therefore, the use of a consensus model, rather than a model based on a single split, is more

DOI: 10.1021/cm504406a
Chem. Mater. XXXX, XXX, XXX−XXX

reasonable. The application of such strategy helps to overcome the problem: the consensus model averages the influence of splits on the modeling results. Moreover, it gives better statistical fit and predictive ability than does the best single model.[8g,19] Similar strategy has been suggested and successfully applied by Gramatica et al.[15a,20]

The plot of the experimental versus predicted values (Figure 3) showed very good agreement between the observed and

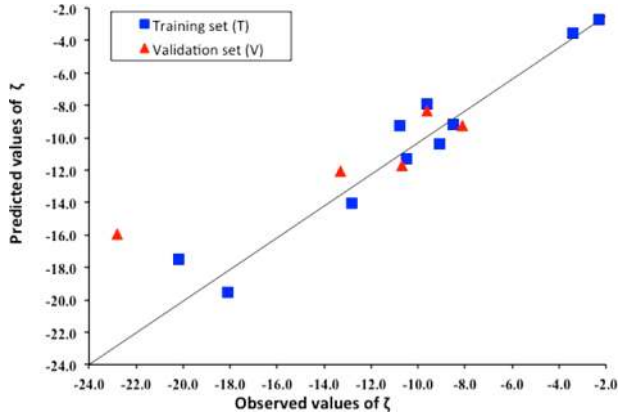

Figure 3. Plot of experimentally observed versus predicted values of zeta potential (ζ) for training and validation compounds.

predicted values of zeta potential for the 15 MeOx-NPs from both the training set and validation set and additionally confirmed the predictive capability of the developed model.

The applicability domain of the best model has been evaluated by the Williams plot (Figure 4). When analyzing the standardized

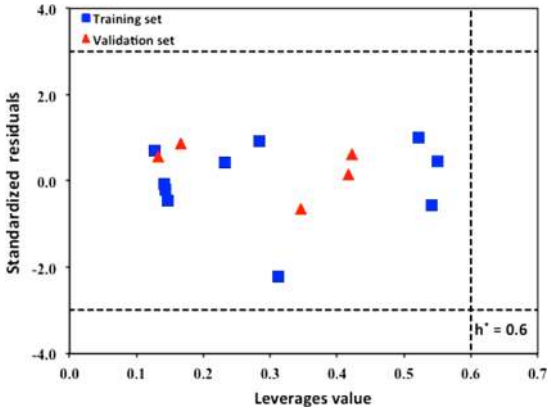

Figure 4. Williams plot for the consensus nano-QSPR model.

residual values ($y^{obs} - y^{pred}$) for the consensus model, we did not observe any outlying predictions (with residuals differing by more than three standard deviations from the average residual value). In addition, none the structures of the studied NPs were substantially different from the training set nanoparticles; all of them were characterized by the leverage values $h_i < h^* = 0.6$. Thus, the model can be successfully applied to predict zeta potential of all studied metal oxides nanoparticles and for other untested metal oxides, if the calculated h_i value is lower than the critical one ($h^* = 0.6$).

However, one should remember that the leverage values h_i used for assessing the applicability domain are calculated from the structural descriptors included in the model, according to the equation

$$h_i = \mathbf{x}_i^{\mathrm{T}}(\mathbf{X}^{\mathrm{T}}\mathbf{X})^{-1}\mathbf{x}_i \tag{13}$$

where $\mathbf{x}_i$ is a row vector of molecular descriptors for ith nanoparticle and $\mathbf{X}$ is a matrix of descriptors for the training set. Thus, they do not include structural variability different than that expressed by the selected descriptors. In consequence, the application of the model, by definition, is restricted to the structures similar to those used for training (i.e., spherical nanoparticles with uncoated surface). As such, it might be inappropriate for other types of nanoparticles (e.g., nanoparticles sterically stabilized by various coatings).

The developed consensus nano-QSPR model is described by eq 14. Please note that the coefficients provided in eq 14 have been derived for the standardized values of descriptors.

$$\zeta = -11.26 - 4.46\psi - 2.39\varepsilon_{\mathrm{HOMO}}/n_{\mathrm{Me}} \tag{14}$$

Interpretation of the descriptors brings significant insight into the current knowledge on structural factors that are likely to affect zeta potential of the studied nanoparticles. The significance of spherical size ψ (standardized coefficient = −4.46) in the model is about two times higher than that of the energy of the highest occupied molecular orbital per metal atom (standardized coefficient = −2.39). Spherical size is inversely proportional to the surface area of the MeOx-NPs, expressed as[21]

$$\psi = \frac{\pi^{1/3}6V^{2/3}}{A} \tag{15}$$

where V is a NP's volume size and A is a NP's surface area. A negative coefficient ψ indicates that the values of zeta potential decrease with the increasing volume (V).[22]

Knowledge of the charge-carrier energy levels on the nanoparticle's surface is essential for understanding an alteration in zeta potential of the particles. Energy of the highest occupied molecular orbital ($\varepsilon_{\mathrm{HOMO}}$) is usually utilized to describe isolated molecules of MeOx (e.g., a single gaseous molecule of TiO_2), and along with Koopman's theorem, it refers to the negative value of their ionization potential. In solid-state particles (i.e., nanoparticles) in which "single molecules" form larger molecular systems, ionization ability can be described by $\varepsilon_{\mathrm{HOMO}}/n_{\mathrm{Me}}$, the HOMO energy weighed by the number of metal atoms (n_{Me}) in a single MeOx unit of the nanoparticle. Because the ability of a given metal oxide to detach electrons (i.e., to form ions on the surface) directly influences the net charge of the whole nanoparticle. The energy of the highest occupied molecular orbital may serve as very informative descriptor.[23] In our model (eq 14), the values of zeta potential of the particles decrease with the increasing $\varepsilon_{\mathrm{HOMO}}/n_{\mathrm{Me}}$ energy.

Interestingly, such descriptors as the energy of the lowest unoccupied molecular orbital, $\varepsilon_{\mathrm{LUMO}}$, and the weighted LUMO energy, $\varepsilon_{\mathrm{LUMO}}/n_{\mathrm{Me}}$, corresponding to electron affinity have not been selected by GA as descriptors that significantly contribute to the model. This means that the formation of cations (positive charge) on the surface of metal oxides is much more favored than the possibility of formation of anions (negative charge). This conclusion is in agreement with various experimental studies.[8d,g,24] The leaching of metal cations from the metal oxide surface and then their interaction with cells is one of the most probable mechanisms responsible for toxicity of metal oxides nanoparticles.

Zeta potential of a nanoparticle is a function of both intrinsic properties of the pristine nanoparticle and parameters describing the environment (temperature, pH, presence of serum, presence

DOI: 10.1021/cm504406a
Chem. Mater. XXXX, XXX, XXX−XXX

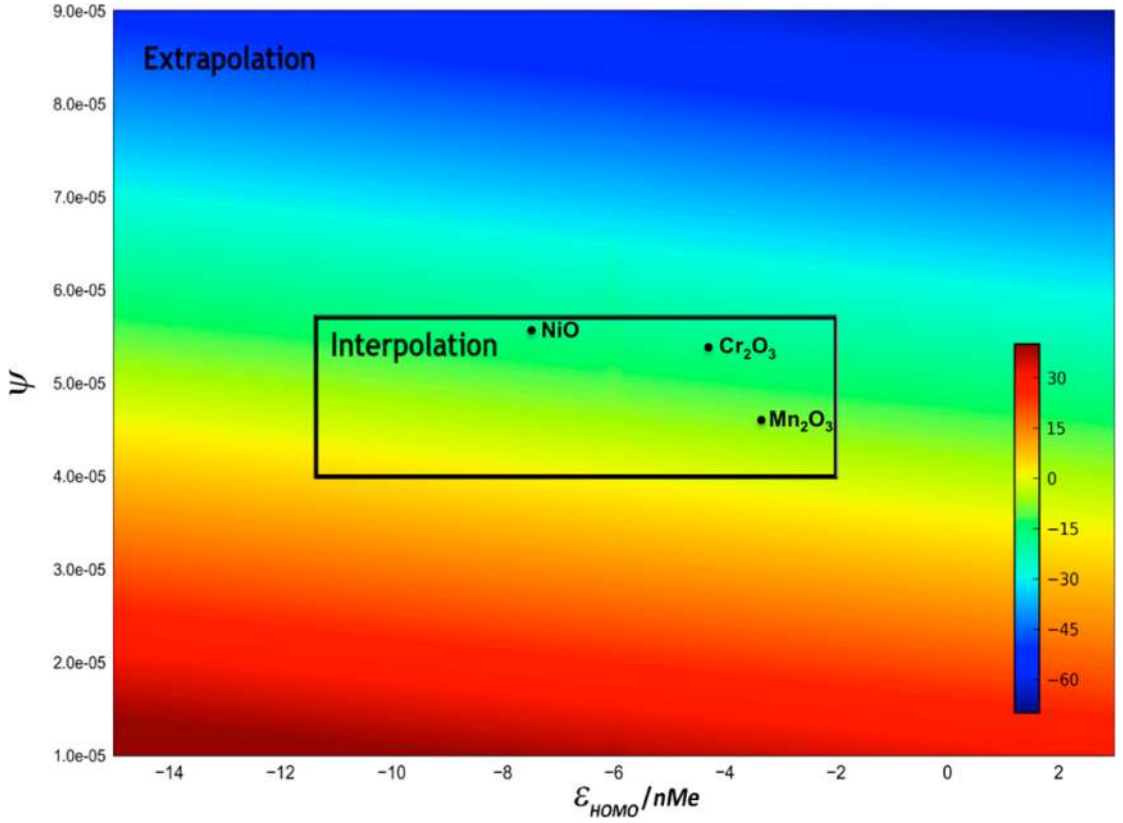

Figure 5. Simulation of zeta potential based on ψ and $\varepsilon_{HOMO}/n_{Me}$ descriptors.

of other compounds, etc.) because they can have influence on the structure, and it is expressed as

$$\zeta = f(\text{intrinsic props of NPs}) + f(\text{environ. params}) \quad (16)$$

In this contribution we have investigated the behavior of nanoparticles assuming that the environmental parameters are the same in case of each studied nanoparticle. We demonstrated that when f (environmental parameters) are constant the values of zeta potential are decreasing with increasing spherical size and the energy of the highest occupied molecular orbital.

There is a logical mechanistic explanation of this conclusion. On one hand, it is known that the ratio between the number of atoms present on the surface area and the number of atoms inside the nanoparticle increases with decreasing particle size. Therefore, small nanoparticles are characterized by a higher mean bond energy per one atom, and in consequence, particular atoms/ions might be much more easily leached from the surface. This leads to the presence of vacancies on the surface; thus, it increases the surface charge. On the other hand, the value of HOMO energy determines the release of electrons and thus ion formation on the surface of particles. Correspondingly, the higher the value of HOMO, the more ionic the forms of atoms present on the nanoparticle surface. Zeta potential represents the charge of the nanoparticle in relation to the surrounding conditions. Therefore, under the same conditions (i.e., when f (environmental parameters) is constant) the surface charge is the only parameter differentiating the values of ζ in the series of metal oxides nanoparticles.

The results obtained in our study, the influence of nanoparticle's structure on zeta potential, are in agreement with the results presented in previously published papers.[1,2b,25] For example, in ref 26, the authors were investigating the electrostatic interaction forces of spherical particles and concluded that spherical radius is one of the important components that influence on zeta potential of these particles. Independently, Berg et al.[25a] showed that the potential influence of metal oxide nature on zeta potential and the effect on agglomeration. This was confirmed by experiment for cases where agglomeration size varies significantly, depending upon a variety factors including both pH and chemical composition. Moreover, in ref 2b, the authors supported the findings that the composition, size, architecture and zeta potential of the nanoparticles are intercorrelated properties. In another work, Powers et al.[25b] discussed the importance of size, chemical composition, and surface charge in the characterization of nanoparticles for toxicological studies and the relationship of these parameters. Authors also confirmed that surface charge is controlled by several mechanisms, including surface ionization, ion adsorption, and lattice ion dissolution.[25b]

In general, solutions with zeta potential of $\zeta < -30$ mV or > +30 mV are considered as very stable.[27] When the value of zeta potential (ζ) tends to 0, the dispersion becomes less stable, and agglomeration/aggregation phenomena occur much easier. As it can be seen, all of the studied MeOx-NPs with values quite close to 0, $\zeta > -30$ mV, actually agglomerate forming species of varying size, when dispersed in cell culture media (Table 1).

Finally, we have applied the model (eq 14) to systematically simulate the values of ζ for different combinations of the descriptors ψ and $\varepsilon_{HOMO}/n_{Me}$. It might be observed (Figure 5) that stable dispersions (under the same the experimental conditions) may exist for nanoparticles having $\psi = 6.0 \times 10^{-5}$ m or greater as well as the energy of the highest occupied molecular orbital between −2 and 0 eV, for $\psi = 6.0 \times 10^{-5}$ m. Moreover, for higher values of $\varepsilon_{HOMO}/n_{Me}$, dispersion can be

DOI: 10.1021/cm504406a
Chem. Mater. XXXX, XXX, XXX−XXX

lower. Note that regarding the ranges of ψ and $\varepsilon_{HOMO}/n_{Me}$ of the training set used for developing the nano-QSPR model the predictions of ζ may be done using either interpolation (within the ranges of the training set) or extrapolation (outside the training set). Although extrapolation is by definition less reliable, the observed trends are clear. Thus, valuable conclusions might also be formulated on the basis of the extrapolated data. The interpolation and extrapolation regions are indicated in Figure 5.

To strengthen the findings of the presented work, we have decided to verify how a proposed heatmap (Figure 5) works for zeta potential (ζ) prediction for three additional MeOx-NPs that were not previously included in the model during developing and testing (namely, NiO, Cr_2O_3, and Mn_2O_3). On the basis of calculated values of ψ and $\varepsilon_{HOMO}/n_{Me}$ descriptors for these three new NPs (Supporting Information, Table S2) and the final model (eq 14), the following values of zeta potential were obtained: −10.47, −16.16, and −16.53, for Mn_2O_3, Cr_2O_3, and NiO respectively. As can be observed in Figure 5, the same values of ζ can be obtained directly from the heatmap. The application of the heatmap presented above may be a suitable computational tool for the preliminary estimation of zeta potential for other MeOx-NPs. It also could be used for the identification of nanomaterials that may tend to be stable within the different range of ζ based only on the calculated values of descriptors.

A nano-QSPR approach might find practical applications in designing new nanoparticles with properties of interest (here zeta potential). However, the predictions based on the currently presented model would be reliable only assuming that (i) the designed structures are similar enough to those used for training the model and (ii) the predicted zeta potential is correct for the same environmental conditions (temperature, presence of serum and other compounds, etc.) as applied when obtaining the experimental data used this study. Further studies should extend the presented model onto different environmental conditions. This, however, requires extensive additional experimental data for calibrating of the model.

CONCLUSIONS

The knowledge of factors that play a prevailing role in zeta potential values of metal oxide nanoparticles is very important. In this study, we have applied a series of computational methods to analyze various factors and to build a model that quantitatively describes the relationship between the zeta potential and the structure of metal oxide nanoparticles (nano-QSPR). The combination of two descriptors(spherical size of nanoparticles and the weighted energy of the highest occupied molecular orbital) show a prominent influence of both structural descriptors on zeta potential (ζ). The finally obtained consensus model is characterized by good predictive power, with Q^2_{EXT} = 0.87. Therefore, the developed model can be recommended for further applications in in silico designing of novel nanoparticles. The proposed nano-QSPR model is the first step in developing a series of computational tools to predict physico−chemical properties of nanoparticles. Predicting intrinsic and extrinsic properties of engineered nanoparticles, such as agglomeration/aggregation phenomena, would in future play an important role in risk assessment of currently used and novel nanomaterials.

ASSOCIATED CONTENT

Supporting Information

Table S1 contains references of necessary crystallographic data utilized to construct the metal oxides clusters, Table S2 shows detailed description of used nanostructural descriptors, Figure S3 shows plots of experimentally observed versus predicted values of zeta potential (ζ) for the training and validation compounds of seven developed nano-QSPR models. This material is available free of charge via the Internet at http://pubs.acs.org.

AUTHOR INFORMATION

Corresponding Author

*E-mail: t.puzyn@qsar.eu.org.

Author Contributions

T.P., A.G., and A.M. conceived the concept; T.P., B.R., and A.M designed the research, analyzed the experimental data, and took part in discussion; A.M. and A.G. prepared calculations; N.S., E.M-G., and S.H. contributed to experimental data; J.L., T.P., and B.R. supervised and directed the project. All authors have given approval to the final version of the manuscript.

Notes

The authors declare no competing financial interest.

ACKNOWLEDGMENTS

This work was supported by the Polish National Science Center (grant no. UMO-2011/01/M/NZ7/01445). The authors also thank for support of the NSF-CREST Interdisciplinary Center for Nanotoxicity (grant no. NSF HRD 0833178 and EPSCoR (award no. 362492-190200-01/NSFEPS-090378). The authors also thank Professor Paola Gramatica for support and for providing a copy of QSARINS software.

ABBREVIATIONS

MeOx-NPs, metal oxide nanoparticles; ζ, zeta potential; ε_{HOMO}, energy of the highest occupied molecular orbital; ψ, spherical size; V, volume; A, surface

REFERENCES

(1) Gajewicz, A.; Rasulev, B.; Dinadayalane, T. C.; Urbaszek, P.; Puzyn, T.; Leszczynska, D.; Leszczynski, J. *Adv. Drug Delivery Rev.* **2012**, *64*, 1663−1693.

(2) (a) Gil, P. R.; Oberdörster, G.; Elder, A.; Puntes, V.; Parak, W. J. *ACS Nano* **2010**, *4*, 5527−5531. (b) Dobrovolskaia, M. A.; McNeil, S. E. *Nat. Nanotechnol.* **2007**, *2*, 469−78.

(3) (a) Gliga, A.; Skoglund, S.; Odnevall Wallinder, I.; Fadeel, B.; Karlsson, H. *Part. Fibre Toxicol.* **2014**, *11*, 11. (b) Limbach, L. K.; Li, Y.; Grass, R. N.; Brunner, T. J.; Hintermann, M. A.; Muller, M.; Gunther, D.; Stark, W. J. *Environ. Sci. Technol.* **2005**, *39*, 9370−9376. (c) Jiang, J.; Oberdörster, G.; Biswas, P. *J. Nanopart. Res.* **2009**, *11*, 77−89.

(4) (a) Murdock, R. C.; Braydich-Stolle, L.; Schrand, A. M.; Schlager, J. J.; Hussain, S. M. *Toxicol. Sci.* **2008**, *101*, 239−253. (b) Lin, D. H.; Tian, X. L.; Wu, F. C.; Xing, B. S. *J. Environ. Qual.* **2010**, *39*, 1896−1908. (c) Schaeublin, N. M.; Braydich-Stolle, L. K.; Maurer, E. I.; Park, K.; MacCuspie, R. I.; Afrooz, A. R.; Vaia, R. A.; Saleh, N. B.; Hussain, S. M. *Langmuir* **2012**, *28*, 3248−58.

(5) (a) Leroy, P.; Devau, N.; Revil, A.; Bizi, M. *J. Colloid Interface Sci.* **2013**, *410*, 81−93. (b) Bouhaik, I. S.; Leroy, P.; Ollivier, P.; Azaroual, M.; Mercury, L. *J. Colloid Interface Sci.* **2013**, *406*, 75−85.

(6) (a) Silva Filho, F. C.; Santos, A. B.; de Carvalho, T. M.; de Souza, W. *J. Leukocyte Biol.* **1987**, *41*, 143−9. (b) Altankov, G.; Richau, K.; Groth, T. *Materialwiss. Werkstofftech.* **2003**, *34*, 1120−1128.

(7) (a) Gramatica, P. *QSAR Comb. Sci.* **2007**, *26*, 694−701. (b) Puzyn, T.; Leszczynska, D.; Leszczynski, J. *Small* **2009**, *5*, 2494−509. (c) Rasulev, B.; Gajewicz, A.; Puzyn, T.; Leszczynska, D.; Leszczynski, J., Nano-QSAR: Advances and Challenges. In *RSC Nanoscience and Nanotechnology*, Puzyn, T.; Leszczynski, J., Eds.; The Royal Society of Chemistry: London, UK, 2012;. (d) Tantra, R.; Oksel, C.; Puzyn, T.; Wang, J.; Robinson, K. N.; Wang, X. Z.; Ma, C. Y.; Wilkins, T. *Nanotoxicology* **2014**, 1−7. (e) Lynch, I.; Weiss, C.; Valsami-Jones, E.

DOI: 10.1021/cm504406a
Chem. Mater. XXXX, XXX, XXX−XXX

Nano Today **2014**, *9*, 266−270. (f) Tropsha, A.; Gramatica, P.; Gombar, V. K. *QSAR Comb. Sci.* **2003**, *22*, 69−77.
(8) (a) Ahmed, L.; Rasulev, B.; Turabekova, M.; Leszczynska, D.; Leszczynski, J. *Org. Biomol. Chem.* **2013**, *11*, 5798−5808. (b) Golbamaki, N.; Avramopoulos, A.; Golbamaki, A.; Rasulev, B.; Cronin, M.; Cassano, A.; Benfenati, E.; Leszczynski, J. *J. Nanomed. Nanotechnol.* **2014**, *5*, 5. (c) Gajewicz, A.; Puzyn, T.; Rasulev, B.; Leszczynska, D.; Leszczynski, J. *Nanosci. Nanotechnol.−Asia* **2011**, *1*, 53−58. (d) Gajewicz, A.; Schaeublin, N.; Rasulev, B.; Hussain, S.; Leszczynska, D.; Puzyn, T.; Leszczynski, J. *Nanotoxicology* **2014**, DOI: 10.3109/17435390.2014.930195. (e) Petrova, T.; Rasulev, B. F.; Toropov, A. A.; Leszczynska, D.; Leszczynski, J. *J. Nanopart. Res.* **2011**, *13*, 3235−3247. (f) Puzyn, T.; Mostrag-Szlichtyng, A.; Gajewicz, A.; Skrzynski, M.; Worth, A. P. *Struct. Chem.* **2011**, *22*, 795−804. (g) Puzyn, T.; Rasulev, B.; Gajewicz, A.; Hu, X.; Dasari, T. P.; Michalkova, A.; Hwang, H. M.; Toropov, A.; Leszczynska, D.; Leszczynski, J. *Nat. Nanotechnol.* **2011**, *6*, 175−8. (h) Rasulev, B.; Leszczynska, D.; Leszczynski, J. In *Advanced Methods and Applications in Chemoinformatics: Research Progress and New Applications*; Castro, E. A., Haghi, A. K., Eds.; IGI Global: Hershey, PA, USA, 2012. (i) Rasulev, B.; Watkins, M.; Theodore, M.; Jackman, J.; Leszczynski, J. *Nanosci. Nanotechnol.−Asia* **2012**, *2*, 2−10. (j) Toropov, A. A.; Toropova, A. P.; Benfenati, E.; Gini, G.; Puzyn, T.; Leszczynska, D.; Leszczynski, J. *Chemosphere* **2012**, *89*, 1098−1102. (k) Toropov, A. A.; Toropova, A. P.; Benfenati, E.; Leszczynska, D.; Leszczynski, J. *Eur. J. Med. Chem.* **2010**, *45*, 1387−1394. (l) Toropov, A. A.; Toropova, A. P.; Puzyn, T.; Benfenati, E.; Gini, G.; Leszczynska, D.; Leszczynski, J. *Chemosphere* **2013**, *92*, 31−37. (m) Kar, S.; Gajewicz, A.; Puzyn, T.; Roy, K.; Leszczynski, J. *Ecotoxicol. Environ. Saf.* **2014**, *107*, 162−169. (n) Kar, S.; Gajewicz, A.; Puzyn, T.; Roy, K. *Toxicol. In Vitro* **2014**, *28*, 600−606. (o) Haranczyk, M.; Urbaszek, P.; Ng, E. G.; Puzyn, T. *J. Chem. Inf. Model.* **2012**, *52*, 2902−9.
(9) Stewart, J. J. P. *MOPAC2009*; Stewart Computational Chemistry: Colorado Springs, CO, 2009. http://OpenMOPAC.net
(10) Sheldrick, G. M. *Acta Crystallogr., Sect. A: Found. Crystallogr.* **2008**, *64*, 112−122.
(11) Cambridge Structural Database in *ConQuest*, version 1.8.
(12) Gramatica, P.; Chirico, N.; Papa, E.; Cassani, S.; Kovarich, S. *J. Comput. Chem.* **2013**, *34*, 2121−2132.
(13) Kutner, M. H. *Applied Linear Regression Models*, 4th ed.; McGraw-Hill/Irwin: New York, 2004.
(14) (a) Holland, J. *Adaptation in Natural and Artificial Systems*; MIT Press: Cambridge, MA, 1992. (b) Devillers, J., Ed. *Genetic Algorithms in Molecular Modeling*; Academic Press: London, 1996.
(15) (a) Chirico, N.; Gramatica, P. *J. Chem. Inf. Model.* **2011**, *51*, 2320−2335. (b) Lin, L. I. K. *Biometrics* **1992**, *48*, 599−604.
(16) Eriksson, L.; Jaworska, J.; Worth, A. P.; Cronin, M. T. D.; McDowell, R. M.; Gramatica, P. *Environ. Health Perspect.* **2003**, *111*, 1361−1375.
(17) Gramatica, P.; Pilutti, P.; Papa, E. *J. Chem. Inf. Comput. Sci.* **2004**, *44*, 1794−1802.
(18) *Guidance Document on the Validation of (Quantitative) Structure-Activity Relationship(Q)SARs Models, ENV/JM/MONO(2007)2*; OECD Environment Health and Safety Publications Series on Testing and Assessment No. 69; a technical report prepared for the Environment Directorate, Organisation for Economic Co-operation and Development: Paris, France, 2007.
(19) (a) Maw, H. H.; Hall, L. H. *J. Chem. Inf. Comput. Sci.* **2001**, *41*, 1248−1254. (b) Pereira, F.; Latino, D. A.; Aires-de-Sousa, J. *J. Org. Chem.* **2011**, *76*, 9312−9319.
(20) Chirico, N.; Gramatica, P. *J. Chem. Inf. Model.* **2012**, *52*, 2044−2058.
(21) Buzea, C.; Blandino, I. I.; Robbie, K. *Biointerphases* **2007**, *2*, MR17−MR172.
(22) Campbell, C. T.; Sharp, J. C.; Yao, Y. X.; Karp, E. M.; Silbaugh, T. L. *Faraday Discuss.* **2011**, *152*, 227−239.
(23) Karelson, M.; Lobanov, V. S.; Katritzky, A. R. *Chem. Rev.* **1996**, *96*, 1027−1044.
(24) (a) Xia, T.; Kovochich, M.; Liong, M.; Mädler, L.; Gilbert, B.; Shi, H.; Yeh, J. I.; Zink, J. I.; Nel, A. E. *ACS Nano* **2008**, *2*, 2121−34. (b) Hu, X.; Cook, S.; Wang, P.; Hwang, H. M. *Sci. Total Environ.* **2009**, *407*, 3070−2. (c) French, R. A.; Jacobson, A. R.; Kim, B.; Isley, S. L.; Penn, R. L.; Baveye, P. C. *Environ. Sci. Technol.* **2009**, *43*, 1354−1359.
(25) (a) Berg, J. M.; Romoser, A.; Banerjee, N.; Zebra, R.; Sayes, C. *Nanotoxicology* **2009**, *3*, 276−283. (b) Powers, K. W.; Palazuelos, M.; Moudgil, B. M.; Roberts, S. M. *Nanotoxicology* **2007**, *1*, 42−51.
(26) Savaji, K. V.; Niitsoo, O.; Couzis, A. *J. Colloid Interface Sci.* **2014**, *431*, 165−175.
(27) Gibson, N.; Shenderova, O.; Luo, T. J. M.; Moseenkov, S.; Bondar, V.; Puzyr, A.; Purtov, K.; Fitzgerald, Z.; Brenner, D. W. *Diamond Relat. Mater.* **2009**, *18*, 620−626.

DOI: 10.1021/cm504406a
Chem. Mater. XXXX, XXX, XXX−XXX